

HT2012-58322

## 2-D SIMULATION OF HOT ELECTRON-PHONON INTERACTIONS IN A SUBMICRON GALLIUM NITRIDE DEVICE USING HYDRODYNAMIC TRANSPORT APPROACH

**Angie Fan**

Advanced Cooling Technologies, Inc  
Lancaster, PA, USA

**Calin Tarau**

Advanced Cooling Technologies, Inc  
Lancaster, PA, USA

**Richard Bonner**

Advanced Cooling  
Technologies, Inc  
Lancaster, PA 17601, USA

**Tomas Palacios**

Massachusetts Institute of  
Technology  
Cambridge, MA, USA

**Massoud Kaviany**

University of Michigan  
Ann Arbor, MI, USA

### ABSTRACT

In this study, a thermal and electrical coupled device solver is developed to simulate the energy transfer mechanism within a GaN FET with a gate length of 0.2  $\mu\text{m}$ . The simulation simultaneously solves a set of hydrodynamic equations (derived from the Boltzmann Transport Equation) and the Poisson equation for electron, optical phonon and acoustic phonon energies, electron number density, electric field and electric potential. This approach has been previously established for gallium arsenide (GaAs) devices [36,37], but has not been extended to GaN due to the lack of readily available property values for GaN devices that are required. Via extensive literature study, high-fidelity properties for GaN were collected in analytical forms with respect to many dependencies, e.g. lattice temperature, electrical field, electron number density, doping rate, defects rate. These properties are then implemented into the developed code to provide a high accuracy sub-micron GaN device simulation.

Simulations show that non-equilibrium heat generation is exhibited in a typical device while the drain current is reduced due to the decrease in electron mobility. Future analysis is needed to quantify the hot-electron effect on reducing the drain current and to discover more effective ways of heat removal.

### INTRODUCTION

Gallium nitride (GaN) structures have outstanding electronic properties. GaN devices operate at higher voltages, higher frequencies, and higher power densities than other devices due to its inherently high critical electric field, electron mobility, and electron saturation velocity. However, the

relatively poor thermal conductivity of GaN and higher heat flux operation make thermal management an issue. Moreover, in sub-micron sized GaN devices, interactions between the electrical and thermal properties become significant due to the strong electron-phonon coupling near the device junction. Therefore, in order to accurately simulate the electrical or thermal performance of a GaN device, the thermal and electrical governing equations need to be solved concurrently.

The thermal energy transfer mechanism near the junction in GaN devices is via scattering of hot electrons with longitudinal optical (LO) phonons, followed by LO-phonon decay to longitudinal acoustic (LA) phonons, which ultimately transport the heat through the substrate. Dissipation of the heat is dominated by the lifetime of LO-phonon. The LO-phonon lifetime is related to electron density, hot electron temperature, and supplied electric power. The strong coupling of electrical and thermal characteristics suggests that GaN properties need to be expressed with many dependencies.

On the device simulation side, most commercially available simulators have been developed over two decades based on Si and GaAs. In the past, the power densities of the devices were not high enough to cause the thermal characteristics to interfere strongly with the electrical behavior. Therefore, the drift-diffusion model was sufficient, which assumes constant temperature while calculating the electrons and holes transport rates. Material properties were also simplified since they were independent of the thermal characteristics. Temperature change was calculated independently using the Fourier's law of heat conduction. These assumptions are no longer valid with the advent of the high-power devices. At high power densities the thermal and

electrical characteristics depend on each other and must be treated as a coupled problem.

The aim of this study is to consider the nonequilibrium nature of the electrons and the phonons and demonstrate the appropriate thermal and electrical characteristics in submicron FETs. We choose MESFET made of GaN for our study due to its simple structure and representation in the signal processing and communication device families.

In section 3, the governing equations of the non-equilibrium semiconductor devices are discussed. Section 4 shows the material properties study. Section 5 discusses the computational method of this work, and Section 6 discusses the results. Finally, Section 7 states the conclusions.

## NOMENCLATURE

$C_p$	Bulk material heat capacity, J/kg-K
$C_{p_A}$	Acoustic phonon heat capacity, J/kg-K
$C_{p_{LO}}$	Optical phonon heat capacity, J/kg-K
$C_{p_{A,mol}}$	Acoustic phonon heat capacity, J/mol-K
$C_{p_{LO,mol}}$	Optical phonon heat capacity, J/mol-K
$E$	Electric field, V/m
$E_c$	Critical electric field, $4.349 \times 10^6$ V/m
$E_L$	Low electric field, $9 \times 10^6$ V/m
$E_H$	High electric field, $3.3 \times 10^7$ V/m
$E_T$	$2.3 \times 10^7$ V/m
$e$	Elementary (electron) charge, $1.60217653 \times 10^{-19}$ C
$h_p$	Planck constant, $6.626 \times 10^{-34}$ J-s
$\hbar$	Reduced Planck constant = $h_p / 2\pi$ , $1.055 \times 10^{-34}$ J-s
$k_B$	Boltzmann constant, $1.381 \times 10^{-23}$ J/K
$k_A$	Acoustic phonon thermal conductivity, W/m-K
$k_e$	Electron thermal conductivity, W/m-K
$m_o$	Electron mass at rest, $9.1 \times 10^{-31}$ kg
$m^*$	Electron effective mass, kg
$N_A$	Avogadro number, $6.022 \times 10^{23}$ mol <sup>-1</sup>
$N_D$	Doping rate, m <sup>-3</sup>
$N_{dis}$	Dislocation rate, m <sup>-2</sup>
$\bar{n}$	Electron number density
$n_{ref}$	Carrier concentration at which the mobility is half way between $\mu_{min}$ to $\mu_{max}$
$Par$	Symbolic parameter in Eq. 10
$Par_o$	Value of the parameter $Par$ at room temperature [1]
$T$	Lattice temperature, K
$v_D$	Electron drift velocity, m/s

$v_{sat,n}$	Electron saturation velocity, m/s
$v_{sat}$	Electron saturation velocity as fitting parameter in Eq. 15, m/s
Greek	
$\alpha_1$	$-2.7182 \times 10^{-10}$ m <sup>3</sup> /V <sup>2</sup> -s
$\alpha_2$	0.0133 m <sup>2</sup> /V-s
$\alpha_3$	$10.54 \times 10^4$ m/s
$\beta_1$	$-2.302 \times 10^{-10}$ m <sup>3</sup> /V <sup>2</sup> -s
$\beta_2$	$9.654 \times 10^{-3}$ m <sup>2</sup> /V-s
$\beta_3$	$1.644 \times 10^5$ m/s
$\Gamma$	Electron-LO phonon scattering rate, s <sup>-1</sup>
$\gamma_1$	$2.096 \times 10^6$ m/s
$\gamma_2$	$1.204 \times 10^{-7}$ m/V
$\gamma_3$	$1.909 \times 10^5$ m/s
$\theta_D$	Debye temperature, K
$\theta_E$	Einstein temperature, K
$\mu_o$	Low field mobility, $0.069$ m <sup>2</sup> /V-s
$\mu_n(E)$	Electron mobility as a function of the longitudinal electric field, m <sup>2</sup> /V-s
$\mu_{n0}$	Low-field electron mobility measured by Hall technique, m <sup>2</sup> /V-s
$\mu_{max}$	Mobility of undoped or unintentionally doped samples where lattice scattering is the main scattering mechanism, m <sup>2</sup> /V-s
$\mu_{min}$	Mobility in highly doped material, where impurity scattering is dominant, m <sup>2</sup> /V-s
$\tau_{e-LO}$	Electron – optical phonon energy relaxation time, s
$\tau_m$	Electron momentum relaxation time, s

## 1. GOVERNING EQUATIONS

The Boltzmann's transport equation (BTE) is valid for general inhomogeneous materials with arbitrary band structure [1]. To solve this equation numerically by discretization of the differential and integral operators in seven-dimensional space is computationally very expensive. A widely used numerical method for solving the BTE is the Monte Carlo (MC) method. This method has been proven to give accurate results, but is still computationally expensive. A good engineering-oriented approach is to transform the BTE into a macroscopic transport model as long as meaningful expressions of electron transport in terms of average electron velocity and effective electron temperature are valid. Blotekjaer (1970) derived conservation equations by taking the moments of the BTE using the weight functions without imposing any assumptions on the form of the

distribution function. The resulting equations represent the electron charge, momentum, and energy conservation, respectively [2]. They are

$$\frac{\partial n}{\partial t} + \nabla \cdot (n\bar{v}) = \left( \frac{\partial n}{\partial t} \right)_c \quad (1)$$

$$\frac{\partial \bar{p}}{\partial t} + \nabla \cdot (\bar{v}\bar{p}) = -en\bar{E} - \nabla \cdot (nk_B T_e) + \left( \frac{\partial \bar{p}}{\partial t} \right)_c \quad (2)$$

$$\frac{\partial W_e}{\partial t} + \nabla \cdot (\bar{v}W_e) = -en\bar{v} \cdot \bar{E} - \nabla \cdot (\bar{v}nk_B T_e) - \nabla \cdot \bar{Q} + \left( \frac{\partial W_e}{\partial t} \right)_c \quad (3)$$

where  $n$  is the electron number density,  $\bar{v}$  is electron drift velocity,  $\bar{E}$  is electrical field, and  $T_e$  is electron temperature.

The electron momentum density  $\bar{p}$  and energy density  $W_e$  can be written as

$$\bar{p} = m^* n \bar{v} \quad (4)$$

$$W_e = 1/2 (3nk_B T_e + m^* n v^2) \quad (5)$$

The last terms in the equations are collision terms. A macroscopic relaxation time approximation is employed to model the collisions as [2]

$$\left( \frac{\partial n}{\partial t} \right)_c = 0 \quad (6)$$

$$\left( \frac{\partial \bar{p}}{\partial t} \right)_c = -\frac{\bar{p}}{\tau_m} = -\frac{m^* n \bar{v}}{\tau_m} \quad (7)$$

$$\left( \frac{\partial W_e}{\partial t} \right)_c = -\frac{w - w_0}{\tau_{e-LO}} = -n \frac{\frac{3}{2} k_B T_e + \frac{1}{2} m^* v^2 - \frac{3}{2} k_B T_{LO}}{\tau_{e-LO}} \quad (8)$$

which introduces the momentum and electron energy relaxation times  $\tau_m$  and  $\tau_{e-LO}$ . A discussion on this approximation is given in [3]. For example, Eq. (6) represents that the electron generation, recombination, and impact ionization in this article are neglected for simplicity. The electron momentum conservation Eq. (2) is the analog of the momentum equation of the Navier-Stokes equations for fluid flow. The driving forces in Eq. (2) are the electric field, the electron number density, and the electron pressure (a.k.a temperature gradients), while the drag force is electron-phonon collision.

For the heat flow vector  $\bar{Q}$  is Eq. (5), the Fourier law is applied,

$$\bar{Q} = -k_e \nabla T_e \quad (9)$$

where  $k_e$  is the electron thermal conductivity. The Fourier law may not be the best way to get a close form. A more accurate method is to consider the third moment of the BTE. But more unknown microscale coefficients such as the relaxation times will be introduced. Under a high electric field  $E > 20$  kV/cm, the electrons become energetic enough to produce optical

phonons. They first lose energy to optical phonons and optical phonons decay to acoustic phonons. The process can be described using the first law of thermodynamics. The resulting energy conservation equations for optical and acoustic phonons are

$$\frac{\partial W_{LO}}{\partial t} = -\left( \frac{\partial W_e}{\partial t} \right)_c + \left( \frac{\partial W_{LO}}{\partial t} \right)_c \quad (10)$$

$$\frac{\partial W_a}{\partial t} = \nabla \cdot (k_a \nabla T_a) - \left( \frac{\partial W_{LO}}{\partial t} \right)_c \quad (11)$$

where  $W_{LO}$  and  $W_a$  are optical and acoustic phonon energy densities, which are related to the heat capacity  $C$  as  $dW = CdT$ , and  $k_a$  is the lattice thermal conductivity. The optical phonon collision in Eq. (10) and Eq. (11) is expressed as

$$\left( \frac{\partial W_{op}}{\partial t} \right)_c = -C_{LO} \frac{T_{op} - T_a}{\tau_{op-a}} \quad (12)$$

where  $\tau_{op-a}$  is optical phonon relaxation time,  $T_{LO}$  and  $T_a$  are the optical and acoustic phonon temperatures. If  $E < 20$  kV/cm, the electrons only interact with acoustic phonons, thus the energy conservation equation become

$$\frac{\partial W_a}{\partial t} = \nabla \cdot (k_a \nabla T_a) - \left( \frac{\partial W_e}{\partial t} \right)_c \quad (13)$$

By applying Eq. (4,5,6,7,8,9,12) into Eq. (1,2,3,10,11) and rearranging the equations, also including the Poisson equation for the electric field, the closed governing equations of the submicron semiconductor devices when  $E > 20$  kV/cm become

$$\nabla^2 V = -\frac{e}{\epsilon_s} (N_D - n) \quad (14)$$

where  $\bar{E} = -\nabla V$

$$\frac{\partial n}{\partial t} - \nabla \cdot (n\mu\bar{E}) - \nabla \cdot \left\{ \frac{\mu}{e} \nabla (nk_B T_e) \right\} = 0 \quad (15)$$

$$\begin{aligned} \frac{\partial T_e}{\partial t} + \nabla \cdot (\bar{v}T_e) &= \frac{1}{3} T_e \nabla \cdot \bar{v} + \frac{2}{3nk_B} \nabla \cdot (k_e \nabla T_e) \\ &+ \frac{m^* v^2}{3k_B} \left( \frac{2}{\tau_m} - \frac{1}{\tau_{e-LO}} \right) - \frac{T_e - T_{LO}}{\tau_{e-LO}} \end{aligned} \quad (16)$$

$$C_{LO} \frac{\partial T_{LO}}{\partial t} = \frac{3}{2} nk_B \frac{T_e - T_{LO}}{\tau_{e-LO}} + \frac{nm^* v^2}{2\tau_{e-LO}} - C_{LO} \frac{T_{LO} - T_A}{\tau_{LO-A}} \quad (17)$$

$$C_A \frac{\partial T_A}{\partial t} = \nabla \cdot (k_A \nabla T_A) + C_{LO} \frac{T_{LO} - T_A}{\tau_{LO-A}} \quad (18)$$

To solve the governing equations numerically, the expressions for the electron mobility, the electron drift velocity, the thermal conductivities for electron and phonons, the heat capacity for the phonons, the momentum and energy relaxation times, and the electron effective mass in GaN are required. An extensive literature study is performed to obtain all the parameters. The results are presented in the following section.

## 2. PARAMETERS

### Optical and acoustic phonon heat capacity

The optical phonon (Einstein) heat capacity and the acoustic phonon (Debye) heat capacity have the following definitions

$$C_{P_{LO,mol}}(T) = 3N_A k_B \left( \frac{\theta_E}{T} \right)^2 \frac{e^{-\frac{\theta_E}{T}}}{(e^{-\frac{\theta_E}{T}} - 1)^2} \quad (19)$$

$$C_{P_{A,mol}}(T) = 9N_A k_B \left( \frac{T}{\theta_D} \right)^3 \int_0^{\frac{\theta_D}{T}} \frac{x^4 e^x}{(e^x - 1)^2} dx \quad (20)$$

where  $N_A$  is the Avogadro number,  $\theta_E$  is the Einstein temperature,  $\theta_A$  is the Debye temperature, and  $T$  is the lattice temperature.

The bulk lattice heat capacity is the sum of both the heat capacities:

$$C_p = C_{P_{LO}} + C_{P_A} \quad (21)$$

The bulk heat capacity is experimentally measurable. The two components,  $C_{P_A}$  and  $C_{P_{LO}}$ , can be found by guessing the characteristic temperatures to fit the experimental bulk value.

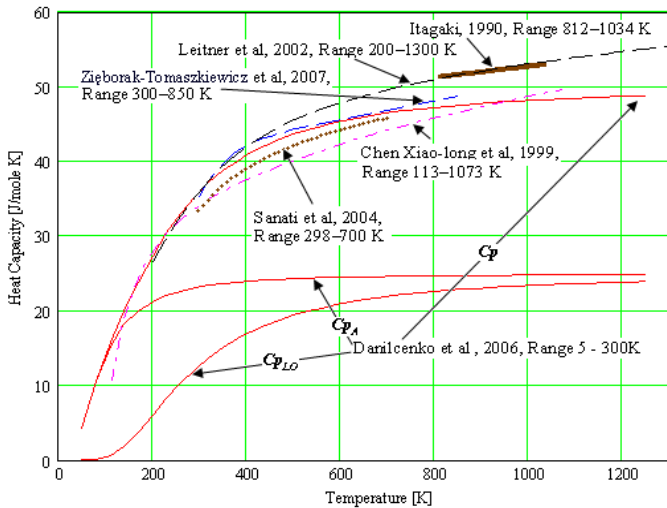


**Figure 1: Optical and acoustic phonon heat capacity fit curve representation validated by bulk GaN heat capacity experimental data.**

In Figure 1, measurements of the bulk lattice heat capacity of the hexagonal GaN by several authors [4,5,6,7,8,9] are

displayed. Danilchenko's measurement was selected for fitting due to the broadest temperature range of 5-300K. The best fit with the accuracy of 3 % was obtained for Debye's temperature  $\theta_A = 365K$  and Einstein's temperature  $\theta_E = 880K$ . The results are shown in Figure 1. The agreement between the experimental data obtained by these authors for the GaN heat capacity and the fit curve based on the sum of the two components (shown as Danilchenko in Figure 1) is reasonable especially in the 100-700 K temperature range. In conclusion, our simulations use Eq. 6 and Eq. 7 for the optical and acoustic phonon heat capacities where  $\theta_D = 365K$  and  $\theta_E = 880K$ .

### Electron drift velocity

The electron velocity in GaN increases for low electric fields and then becomes quasi-saturated close to 20 kV/cm<sup>10</sup>. After this quasi-saturation, the electron velocity increases again, reaching a maximum for an electric field of 100 kV/cm and then it decreases to its saturated value of  $1.2 \times 10^7$  cm/s. A very important difference between the high field transport model of GaN and that of other semiconductors is that in the latter, there is no quasi-saturation of the electron velocity. The quasi-saturation behavior is generally associated with the onset of optical phonon emission in nitride based semiconductors [11,12]. In other semiconductors like Si or GaAs, the energy for optical phonon emission is much lower and the quasi-saturation is not very different from the standard saturation. Some authors have also associated the early saturation of the electron velocity in AlGaIn/GaN structures with hot phonon scattering [13,14]. It is obvious that the need for a valid GaN electron transport model under high electric field is significant and literature offers both experimental and simulation data [15,16,17,18,19,20,21,22,23,24,25,26,27].

Schwierz (2005) proposed a complete analytical model for the electron mobility in wurtzite GaN.

$$v(E) = \frac{\mu_o E + v_{sat} \left( \frac{E}{E_c} \right)^{n_1}}{1 + \left( \frac{E}{E_c} \right)^{n_1} + n_2 \left( \frac{E}{E_c} \right)^{n_3}} \quad (22)$$

$$\mu_o = \mu_{min} + \frac{\mu_{max} - \mu_{min}}{1 + \left( \frac{n}{n_{ref}} \right)^\alpha} \quad (23)$$

where  $\mu_o$  is the low-field mobility,  $v_{sat}$ ,  $E_c$ ,  $n_1$ ,  $n_2$ ,  $n_3$ ,  $\mu_{min}$ ,  $\mu_{max}$ ,  $n_{ref}$  and  $\alpha$  are fitting parameters.  $\mu_{max}$  represents the mobility of undoped or unintentionally doped samples where lattice scattering is the main scattering mechanism.  $\mu_{min}$  is the mobility in highly doped material, where impurity scattering is dominant. The parameter  $\alpha$  is a

measure of how quickly the mobility changes from  $\mu_{\min}$  to  $\mu_{\max}$ .  $n_{ref}$  is the carrier concentration at which the mobility is half way between  $\mu_{\min}$  to  $\mu_{\max}$ . The temperature dependence of the low-field mobility can be modeled by making the four fitting parameters in Eq. 23 temperature dependent according to

$$Par(T) = Par_o \times \left( \frac{T}{300K} \right)^{\gamma(Par)} \quad (24)$$

where  $Par$  is the parameter of interest (i.e.  $\mu_{\min}$ ,  $\mu_{\max}$ ,  $n_{ref}$  and  $\alpha$ ),  $Par_o$  is the value of the parameter  $Par$  at room temperature. For the rest parameters  $v_{sat}$ ,  $E_c$ ,  $n_1$ ,  $n_2$ ,  $n_3$  in Eq. 22, the temperature dependent relationship can be derived by

$$Par(T) = Par_o \times (a + bT + cT^2) \quad (25)$$

where a, b, and c are constants that have to be determined by fitting.

Through a series development of the parameters, the final expression for the drift velocity and the electron mobility become

$$v(E, n, T) = \frac{\mu_o(n, T)E + v_{sat}(T) \left( \frac{E}{E_c(T)} \right)^{n_1(T)}}{1 + \left( \frac{E}{E_c(T)} \right)^{n_1(T)} + n_2(T) \left( \frac{E}{E_c(T)} \right)^{n_3(T)}} \quad (26)$$

$$\mu(E, n, T) = \frac{\mu_o(n, T) + v_{sat}(T) \left( \frac{E}{E_c(T)} \right)^{n_1(T)-1}}{1 + \left( \frac{E}{E_c(T)} \right)^{n_1(T)} + n_2(T) \left( \frac{E}{E_c(T)} \right)^{n_3(T)}} \quad (27)$$

$$\mu_o(n, T) = \mu_{\min} \left( \frac{T}{300K} \right)^{-0.2} + \frac{\mu_{\max} \left( \frac{T}{300K} \right)^{-2.85} - \mu_{\min} \left( \frac{T}{300K} \right)^{-0.2}}{1 + \left( \frac{n}{n_{ref} \left( \frac{T}{300K} \right)^{1.3}} \right)^{\alpha \left( \frac{T}{300K} \right)^{0.31}}} \quad (28)$$

where

$$\begin{aligned} v_{sat}(T) &= v_{sat\_300K} \left[ 0.94475 + 5.5183 \times 10^{-4} T - 1.2256 \times 10^{-6} T^2 \right] \\ E_c(T) &= E_{c\_300K} \left[ 0.8604 + 3.88 \times 10^{-4} T + 2.5778 \times 10^{-7} T^2 \right] \\ n1(T) &= n_{1\_300K} \left[ 1.099 - 3.1373 \times 10^{-4} T - 5.28 \times 10^{-8} T^2 \right] \\ n2(T) &= n_{2\_300K} \left[ 3.99 - 1.338 \times 10^{-2} T + 1.1373 \times 10^{-5} T^2 \right] \\ n3(T) &= n_{3\_300K} \left[ 1.211 - 1.52 \times 10^{-3} T + 2.727 \times 10^{-6} T^2 \right] \\ v_{sat\_300K} &= 1.27 \times 10^7 \text{ cm/s} \\ E_{c\_300K} &= 172 \text{ kV/cm} \\ n_{1\_300K} &= 4.19 \\ n_{2\_300K} &= 3.24 \\ n_{3\_300K} &= 0.885 \end{aligned}$$

#### Thermal conductivity – phonon and electron

Thermal conductivity of GaN mainly consists of two components:  $k_A$  – the acoustic phonon thermal conductivity (or lattice thermal conductivity) and  $k_e$  – the electron thermal conductivity.

In a theoretical investigation [28] of the thermoelectric effects in wurtzite GaN crystals the two main contributions to the GaN thermal conductivity were evaluated. The dependence of the phonon contribution ( $k_A$ ) to the thermal conductivity on the dislocation and point defect densities has been studied in detail by Zou [29] and co-workers [30]. It has been established that the room temperature thermal conductivity in wurtzite GaN is sensitive to the dislocation line density  $N_{dis}$  only for very large values of  $N_{dis} > 5 \times 10^{10} \text{ cm}^{-2}$ . At this high dislocation range the variation of the dislocation line density by two orders of magnitude can bring about a large (factor of two) variation in the thermal conductivity value. For GaN materials with lower dislocation density, the room temperature thermal conductivity is more sensitive to the

concentration of point defects impurities, dopants, etc. For example, the change in the doping density can lead to a variation of  $k_A$  from 1.77 W/cm-K to 0.86 W/cm-K at 300 K. In their work they selected  $N_{dis} = 5 \times 10^{10} \text{ cm}^{-2}$  and determined  $k_A$  from the virtual-crystal model [31]. It is well known that the  $k_A$  contribution is much larger than  $k_e$  for most practical situations even at very large doping densities.

$$k_A(T) = \begin{cases} a_4 T^4 + a_3 T^3 + a_2 T^2 + a_1 T + a_0 & \text{if } T \leq 30K \\ b_5 T^5 + b_4 T^4 + b_3 T^3 + b_2 T^2 + b_1 T + b_0 & \text{if } 30K < T \leq 80K \\ c_1 T^{c_2} & \text{if } 80K < T \leq 1000K \end{cases} \quad (29)$$

where:

$$\begin{aligned} a_0 &= 389.29 & b_0 &= -56323.56 \\ a_1 &= -306.23 & b_1 &= 6033.772 \\ a_2 &= 73.421 & b_2 &= -213.4318 \\ a_3 &= -2849826 \times 10^{-6} & b_3 &= 35072 \times 10^{-4} \\ a_4 &= 33009 \times 10^{-7} & b_4 &= -27691 \times 10^{-6} & c_1 &= 402946 \\ & & b_5 &= 852 \times 10^{-7} & c_2 &= -1.3778 \end{aligned}$$

For  $N_{dis} = 10^6 \text{ cm}^{-2}$  and  $N_{dis} = 10^8 \text{ cm}^{-2}$ , we have:

$$k_e(T) = d_2 T^2 + d_1 T + d_0 \quad (30)$$

For  $N_{dis} = 10^{10} \text{ cm}^{-2}$  we have:

$$k_e(T) = f_3 T^3 + f_2 T^2 + f_1 T + f_0 \quad (31)$$

where:

$$\begin{aligned} d_0 &= -0.00163 & f_0 &= 471 \times 10^{-5} \\ d_1 &= 0.0002 & f_1 &= -904 \times 10^{-7} \\ d_2 &= 0.1885 \times 10^{-6} & f_2 &= 504 \times 10^{-9} \\ & & f_3 &= -127 \times 10^{-12} \end{aligned}$$

Eq. 29~31 are used in our device simulator. It is observed that electron number density is not among the dependencies for the thermal conductivity of the electron. However, it is shown (Liu-2005) that electron thermal conductivity becomes a significant contribution for the overall GaN thermal conductivity only for doping rates larger than  $10^{19} \text{ cm}^{-3}$ . Since in our simulations the doping rates are smaller, the lack of electron number density as dependency is not a concern.

#### Electron effective mass

Various methods were used to find the effective mass of the electron in GaN and the resulted electron effective mass considered in our device simulator for GaN is:

$$m^* = 0.21 m_o \quad (32)$$

where  $m_o = 9.1 \times 10^{-31} \text{ kg}$  is the electron mass at rest.

#### Electron momentum relaxation time

The electron momentum relaxation time can be calculated from the relation [32]

$$\tau_m = \frac{\mu m^*}{e} \quad (33)$$

Since the electron mobility is a function of electric field, electron number density and temperature (as seen in Eq. 27), the electron momentum relaxation time  $\tau_m$  will have the same dependencies and the analytical representation is:

$$\tau_m(E, n, T) = \frac{\mu(E, n, T) \cdot 0.21 m_o}{e} \quad (34)$$

where  $\mu(E, n, T)$  is the electron mobility described by Eq. 27.

#### Electron- optical phonon energy relaxation time

Electron-longitudinal optical phonon scattering rates in wurtzite GaN have been directly measured [33] by sub-picosecond time-resolved Raman spectroscopy. It was found that the total electron-LO phonon scattering rate is given by  $\Gamma = (4 \pm 0.8) \times 10^{13} \text{ s}^{-1}$ . Since the electron-LO phonon scattering rate is about  $\Gamma = 5 \times 10^{12} \text{ s}^{-1}$  in GaAs [34] the observed total electron-LO phonon scattering rate in GaN is almost one order of magnitude larger than that in GaAs. One of the possible explanations for this enormous increase of electron-LO phonon scattering rate in GaN is its much larger ionicity as reflected from the much larger LO-TO phonon splitting. In general, the strength of the electron-LO phonon coupling is set by the lattice-dipole interactions. This splitting is directly proportional to the lattice polarization, and is a measure of the effective charge. In GaAs, the LO-TO splitting is about 3 meV, while it is about 25 meV in wurtzite GaN. However, in the two-mode system of hexagonal GaN, this must be split between the two modes to compute the contribution of each of the dielectric function. This together with the much smaller dielectric constant of GaN, lead to an expected increase of a factor of 9 in the scattering strength, which is quite close to that observed experimentally. It is estimated [35] that the effective charge of GaN is about twice that of GaAs, while the dielectric constant is almost half. These two factors above would suggest a factor of 8 increase in the electron-LO phonon scattering strength. This provides a consistent interpretation of the scattering increase as due to the ionicity of GaN relative to GaAs. In conclusion, the total electron-LO phonon scattering time is:

$$\tau_{e-LO} = 0.025 \pm 0.042 \text{ ps} \quad (35)$$

### 3. NUMERICAL STUDY OF A SUB-MICRON GAN MESFET

Metal-semiconductor field-effect transistors (MESFET) Figure 2 are usually made of III-V materials and commonly used in high-speed communication devices. Heat generation and transport in gallium arsenide (GaAs) MESFETs using the hydrodynamic method has been studied [36,37]. In this work, the heat generation and transport in 2D GaN MESFET with the updated properties is presented.

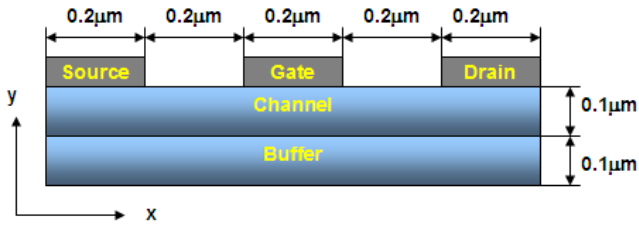


**Figure 2: Two-dimensional metal-semiconductor field-effect transistor (MESFET) structure for computation**

The computational domain of the 2D transistor is shown in Figure 2. Finite difference method is used to discretize the set of governing equations. Second order central difference scheme is applied to all terms except for the second term on the left-hand side of Eq. 16, where a first-upwind scheme is applied. Square mesh is applied to the entire domain with a uniform grid size of 5 nm. A constant voltage is applied between the drain and source contacts. Zero voltage and a Schottky barrier height  $\phi_B = -0.8V$  are applied on the gate contact. At the rest of the boundary, zero gradient normal to the boundary is used. For electron number density  $n = N_D$  is used at each of the source and the drain contacts, and zero particle flux normal to the boundary is applied at the rest of the boundary. For LO-phonon and acoustic phonon temperatures, constant heat transfer coefficient  $h = 10^3 W/m^2 - K$  is given at the top and bottom boundaries. At the rest boundaries, an adiabatic condition is applied to simulate the shoulder to shoulder chip packaging arrangement. For electron temperature, an adiabatic condition is applied to the entire boundary. Implicit time-marching scheme is applied for all five equations. The LU Decomposition Conjugate Gradient Squared (LUCGS) method is used to solve the matrix. Two time steps of 0.01 ps and 4.5 ps are used for iteration. The first time step is used at the beginning of the iteration when the electron temperature responds rapidly to the applied field. Once the electron temperature reaches a quasi-steady state with very little change, a larger time step is used.

### 4. RESULTS AND DISCUSSIONS

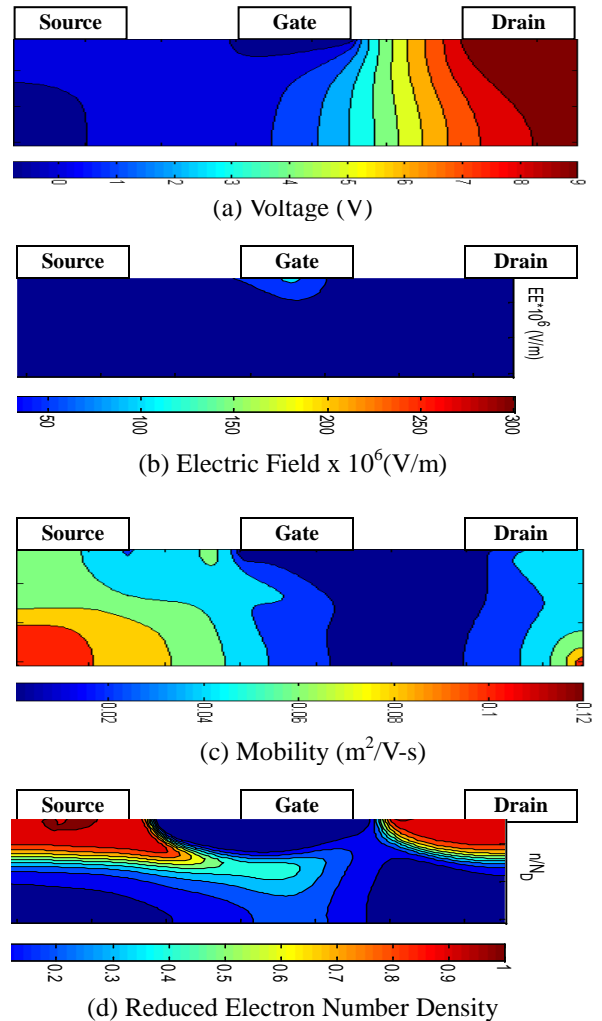
Figure 3 gives the computational results for the voltage, electric field, electron mobility and reduced electron number density in the GaN device where  $V_{sd}=10V$ ,  $V_g=0V$ ,  $t=17ps$ .

Figure 3(a) shows the voltage distribution. Although there is no voltage applied to the gate contact, underneath the gate

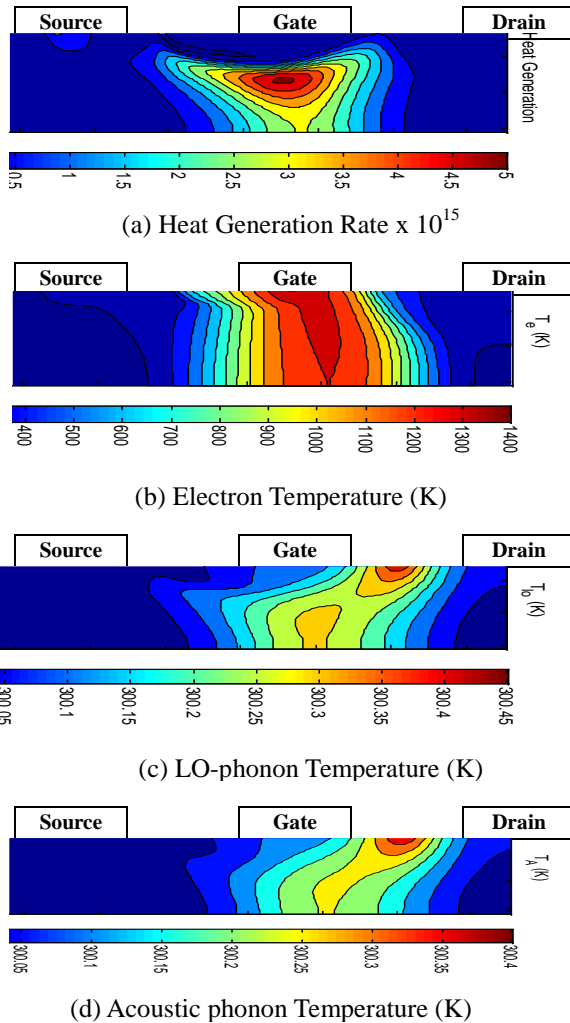
there is a narrow zone of negative potential. This is due to the Schottky barrier. It is also shown that the major voltage drop occurs at the drain side, which means higher electric field will occur in this region. This is confirmed by the plot of the electric field distribution, Figure 3(b). The highest electric field locates under the gate at the drain side.

Figure 3(c) shows the computed profile of the electron mobility. There is a large zone of low mobility under the gate and drain. This zone coincides with the major voltage drop zone in Figure 3(a). The physics behind this is that the strong hot-electrons and LO-phonons scattering occurring in this region due to the extremely high electric field makes the electron velocity saturate. The electron mobility model adopted here depends not only on the average energy but also on the electric field and the electron number density; therefore it prevents the velocity overshoot [1] in the non-equilibrium device.

Figure 3(d) shows the reduced electron number density  $n/N_D$ . A wide depletion zone is clearly shown under the gate. Therefore, the current channel is narrow which leads to large current density.



**Figure 3 Calculated electrical characteristics in GaN device**



**Figure 4** Calculated thermal characteristics in GaN device

Figure 4 shows the concurrently computed heat generation rate, electron temperature, LO-phonon temperature and acoustic phonon temperature.

Figure 4(a) shows the heat generation rate. The heat generation rate is the product of the current density and the electric field. The current density and the electric field in the gate channel at the drain side are higher; therefore the highest heat generation rate appears around the region.

Figure 4(b) shows the distribution of the electron temperature. The hot electrons appear under the gate at the drain side corresponding to the high electric field. The peak electron temperature is 1400 K. The electron temperatures in the rest of the devices remain around 300 K. Experimental measurement is needed for verification.

Figure 4(c) (d) show the LO-phonon and acoustic phonon temperatures. The highest temperature region appears under the drain. Comparing to the electron temperature, the two lattice temperatures rise much slower. For the given computing time ( $t=17\text{ps}$ ), the lattice temperatures are slightly increased. It is understandable that the electrons pick up the energy much more

efficient from the applied electric field than transfer the energy to the lattice. But experimental data need to be compared in the future work.

## 5. CONCLUSIONS

In this work, a 2-D hydrodynamic equations based GaN device simulator is established to capture the coupling effects of the electrical and thermal characteristics in high power GaN devices. High fidelity material properties are established from an intensive literature study. It reveals the unique electron transfer feature in GaN. Future work includes validate the simulator with broad experimental data, improve the computational efficiency, and discover more effective ways of heat removal

## ACKNOWLEDGMENTS

This work was supported by the National Reconnaissance Office's (NRO) Applied Technology Department (ATD) through the Jalapeno program under contract NRO00-09-C-0348.

## REFERENCES

- [1] Tibor Grasser, Ting-wei Tang, Hans Kosina, and Siegfried Selberherr, "A Review of Hydrodynamic and Energy-Transport Models for Semiconductor Device Simulation", *Proceedings of the IEEE*, vol. 91, No. 2, Feb. 2003
- [2] Jie Lai, and Arun Majumda, "Concurrent Thermal and Electrical Modeling of Submicrometer Silicon Devices", *J. Appl. Phys.* 79 (9), 1May 1996
- [3] M. Lundstrom, Fundamentals of Carrier Transport. Reading, MA:Addison-Wesley, vol. 10, *Modular Series on Solid State Devices*, 1990
- [4] Danilchenko, B. A. , T. Paszkiewicz, S. Wolski, A. Jeżowski, and T. Plackowski, "Heat capacity and phonon mean free path of wurtzite GaN", *Appl. Phys. Lett.* 89, 2006
- [5] Chen, X., Lan, Y., Liang, J., Cheng X., Xu Y., Xu T., Jiang P., and Lu K., "Structure and Heat Capacity of Wurtzite GaN from 113 to 1073 K", *Chinese Phys. Lett.* 16, 1999
- [6] Itagaki, K. et.al., *Thermochim. Acta*, 163, 1990
- [7] Leitner, J., Strejc, A., Sedmidubský, D., Růžička, K., "High temperature enthalpy and heat capacity of GaN", *Thermochimica Acta*, Volume 401, Issue 2, Pages 169–173, 2003
- [8] Ziborak-T I., et.al., *Journal of Thermal Analysis and Calorimetry*, 91, 2008
- [9] Sanati, M., Albers, R. C., and Pinski, F. J., "ω-phase formation in NiAl and Ni<sub>2</sub>Al alloys", *J. Phys.: Condens. Matter* 13, 2001
- [10] Palacios T. et.al. *Nitride Semiconductor Devices*, Piprek, 2007
- [11] Singh M., *J. Appl. Phys.* 94, 2003
- [12] Gelmont B., *J. Appl. Phys.* 74, 1993
- [13] Ardaravicius L. et.al. *Appl.Phys.Lett.*83, 2003
- [14] Ridley B.K. et.al., *J. Appl. Phys.* 96, 2004

- 
- [15] Caughey D.M., et.al., *Proc. IEEE* 55, 1967
- [16] Benbakhti B. et. al., *J. Phys.* 193, 2009
- [17] Kabra S. et.al. *Microelectronics Journal* 37 2006
- [18] Schwierz F., *Solid-State Electronics* 49, 2005
- [19] Mnatsakanov T.T., et. al. *Solid-State Electron*, 47, 2003
- [20] Farahmand M., et.al. *Solid-State Electronics*, 49, 2005
- [21] Arora N.D. et.al. *IEEE Trans Electron Dev*, 29, 1982
- [22] Farahmand M., et.al. *Solid-State Electronics*, 49, 2005
- [23] Schwierz F.: A compilation of more than 200 references. 2004
- [24] Look D.C., et.al. *Appl Phys Lett*, 79, 2001
- [25] Schwierz F., *Solid-State Electronics*, 49, 2005
- [26] Mnatsakanov T.T., et. al. *Solid-State Electron*, 47, 2003
- [27] Farahmand M., et.al. *Solid-State Electronics*, 49, 2005
- [28] Liu W., et al., *J. Appl. Phys.* 97, 2005
- [29] Zou J., et al., *J. Appl. Phys.* 92, 2002
- [30] Kotchetkov D., et al., *Appl. Phys. Lett.* 79, 2001
- [31] Liu W., et.al., *Appl. Phys. Lett.* **85**, 2004
- [32] Kittel, 1986
- [33] Tsen K.T., et. al., *Appl. Phys. Lett.*, 71, 1997
- [34] Kash, J. A. , et al. *Phys. Rev. Lett.* 54, 1985
- [35] Phillips, J. C., et.al. *Bands in Semiconductors ~Academic*, New York, 1973
- [36] Majumdar A., Fushinobu K., and Hijikata, K., “Effect of gate voltage on hot-electron and hot-phonon interaction and transport in a submicrometer transistor”, *J. Appl. Phys.*, 21, 1995
- [37] Fushinobu K., Majumdar, A., and Hijikata, K., “Heat generation and transport in submicron semiconductor devices”, *J. of Heat Transfer*, 31, 1995